Pergamon

Journal of Structural Geology, Vol. 20, No. 9/10, pp. 1205 to 1218, 1998

0191-8141/98/$ - see front matter

PII: S0191-8141(98)00064-9

Modeling the thermal evolution of fault-controlled magma emplacement models: implications for the solidification of granitoid plutons

AARON S. YOSHINOBU*, DAVID A. OKAYA and SCOTT R. PATERSON

Department of Earth Sciences, University of Southern California, Los Angeles, CA 90089-0740, U.S.A.

(*Received* 1 *July* 1997; *accepted in revised form* 20 *April* 1998)

Abstract—A two-dimensional finite difference model is used to simulate the conductive thermal regime attending construction and maintenance of a continental magma chamber by intrusion of granite dikes into granodiorite host rocks displaced at various spreading rates. Final intrusion shapes include tabular, square, and vertical rectangular bodies emplaced in the shallow crust (5–15 km) and tabular bodies emplaced in the middle crust (15–20 km) fed by dikes with widths of between 20 and 100 m. The formation of a steady-state chamber is defined as the point at which the ambient temperatures surpass the intrusion solidus forestalling the solidification of subsequently intruded material. For spreading rates < 10 mm year^{-1}, construction of a steady-state magma chamber in the shallow crust took 260 ka (rectangular), 360 ka (square), and 1 Ma (tabular), whereas in the mid crust a steady state was reached in less than 30 ka (tabular). At faster spreading rates (25 and 50 mm year^{-1}) ambient temperatures pass the solidus isotherm forming a steady-state reservoir within 55 ka, depending on intrusion depth and size. For 10–25 mm year^{-1} spreading rates, sheeted dikes make up from 10 to 100% of the intrusion.

The thermal modeling supports the following conclusions: (a) episodic magma emplacement into a fault-controlled setting is a thermally viable means of constructing a steady-state chamber at moderate to fast spreading rates only if the duration of faulting and intrusion are long enough to elevate ambient temperatures above the intrusion solidus, (b) isotherms will migrate outward during successive intrusion before converging back on the center of the intrusion after chamber construction, (c) the margins of most intrusions formed by this scenario should contain sheeted dikes, (d) the solidus isotherm, and thus the solidification front that it tracks, will become progressively curviplanar during the construction of the magma chamber and will not represent the initial shape of the intrusions (i.e. sheets), (e) the steady-state chamber will be smaller than the total intrusion dimensions, and (f) magmatic fabrics will form diachronously and not always parallel to sheet margins as they track the migrating solidification front. Because it is unlikely that most large intrusions formed instantaneously, the effects of continued addition of heat on the migration of solidification fronts may have significant implications for magmatic processes in many emplacement scenarios.

INTRODUCTION

The ascent and emplacement of magmas is the principal means by which heat and mass are transferred into and through the Earth's crust. Hutton (1794) first recognized the intrusive nature of granitic bodies and Read (1962) alluded to the thermal and mechanical coupling between intrusion and host rocks as magma is transferred through the crust. Understanding the coupling between the processes of magma ascent, emplacement, and host rock displacement is of first order importance in relating magmatism to volcanic arc or ocean crust formation. For example, given that the magma ascent rate in dikes may be many orders of magnitude faster than other ascent mechanisms, an implication is that the construction rates of continental magma chambers—i.e. the displacement rate of the host rocks—must be compatible with the volume of magma added at the emplacement level. Therefore, it is critical to evaluate whether the rate of host rock displacement by different processes is sufficient to construct a large magma chamber.

One model for coupled host rock displacement and magma emplacement in magmatic arc settings involves intrusion into a fault-controlled reservoir (e.g. Guineberteau *et al*., 1987; Hutton, 1988a, b; Schmidt *et al*., 1990; Tikoff and Teyssier, 1992; Karlstrom *et al*., 1993; Grocott *et al*., 1994; Ferre *et al*., 1995). In this model, magma is emplaced via dikes into a releasing bend separating en échelon strike-slip faults (Fig. 1). Other fault-controlled scenarios include the extensional terminations of strike-slip faults (e.g. Strontian granite, Hutton, 1988a), extensional duplexes (e.g. plutons of the Mid-Mesozoic Andean margin of northern Chile, Grocott *et al*., 1994), and local extension in contractional duplexes (e.g. Boulder and Tobacco Root batholiths, Schmidt *et al*., 1990). During continued displacement, successive batches of magma are added to the growing reservoir presumably as dikes, supplying additional heat to the system.

Two conditions must be met in order for large, unsheeted, typically zoned plutons with chamber-wide magmatic foliation patterns to be emplaced by a fault-controlled model in continental settings (e.g. Tikoff and Teyssier, 1992). First, there must be a sufficient magma supply in the source region (Petford, 1996). If not, a low magma supply would require long periods

*E-mail: yoshinob@earth.usc.edu

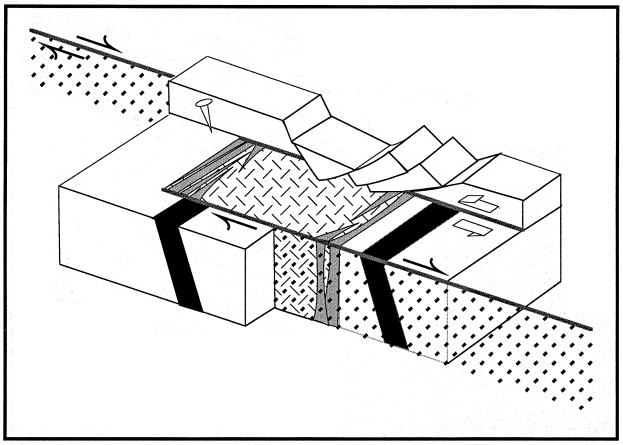

Fig. 1. Schematic, three-dimensional illustration of the fault-controlled emplacement model displaying characteristics that may be observed in the field including: extended and/or detached roof, retrodeformable host rock markers (tilted black layer), sheeted igneous rocks along the margins, and large displacement syn-emplacement faults (diagonal, dotted lines).

between intrusion thus allowing individual dikes to cool. Second, the rate of heating by successive intrusions must be greater than cooling so that the ambient temperature in the chamber is elevated above the magma solidus. If this occurs, a stable chamber (i.e. a chamber in which temperature remains above the solidus) will be maintained in which magmatic processes, such as flow, fractionation, and interaction with adjacent magmas, can potentially occur. If both conditions are not met during successive dike emplacement, then construction and maintenance of a steady-state magma chamber cannot occur and a sheeted dike complex analogous to those found in ophiolites should result (Sleep, 1975). We assume for modeling purposes that a sufficient magma supply is available during each slip event and under this condition contend that the rate-controlling step in elevating ambient temperatures above the solidus is the slip rate on the chamber bounding faults. These slip rates control how fast host rock is displaced and thus how fast magma (and thus heat) can be transported to the part of the crust under consideration.

Thermal models provide a means of evaluating the intensive parameters that affect such emplacement models, and numerical tests have been developed to evaluate the thermal behavior during coeval magma emplacement and host rock displacement (e.g. Hanson and Glazner, 1995). We have developed a two-dimensional finite difference numerical model to evaluate the thermal conditions during construction and maintenance of a magma chamber by extension. The advantages of the finite difference method over earlier analytical conduction models (e.g. Jaeger, 1968) is that spatial and temporal variations in host rock and intrusion properties, intrusion geometry, and intrusion depth can be evaluated. Our intrusion rate-dependent thermal modeling is modified from the one-dimensional and two-dimensional finite difference thermal conduction methods of Furlong *et al.* (1991) to allow for (a) episodic, rather than instantaneous addition of intrusive material, (b) mechanical translation of host rocks and older dikes, and (c) temporally and spatially varying physical properties of the magma–host rock system such as geothermal gradient, latent heat, and rock properties. Our modeling also differs from previous models in that intrusion is controlled by discrete faulting events which govern the size of individual intrusions rather than a conduit(s) that continuously feeds the growing magma chamber.

Our results indicate that fault-controlled magma emplacement models are thermally viable means of constructing intrusions of the dimensions typically found in dissected magmatic arcs or collisional belts only if (a) the duration of faulting is long enough to allow sufficient time to elevate the ambient temperatures above the intrusion solidus, and (b) for geologically reasonable slip rates, margins of the intrusions are sheeted (e.g. Fig. 1). The thermal simulations also indicate that the active (magmatic) portion of the chamber will be smaller than the total intrusion at a given time and that magmatic fabrics, which form at the solidification front, will form diachronously. Because it is unlikely that large plutons are constructed instantaneously, we contend that effects of successive additions of heat on the evolution of solidification may also have important implications for magmatic processes in other emplacement scenarios (e.g. nested intrusions, laccoliths).

TWO-DIMENSIONAL MODELS OF CONDUCTIVE HEAT TRANSFER

Review of previous analytical and numerical thermal models

Earlier analytical and numerical modeling (e.g. Jaeger, 1968; Bowers *et al.*, 1990; Furlong *et al.*, 1991) assumed instantaneous intrusion of an igneous body and therefore did not evaluate the time-dependent transient thermal effects on the host rocks of a growing intrusion. Sleep (1975) first presented an analytical solution for the two-dimensional steady-state thermal structure of an oceanic spreading center magma chamber involving mass (heat) addition commensurate with extension. For rates of spreading >10 mm year^{-1}, the increased heat provided by mass addition was sufficient to maintain a chamber of magma or crystal-melt mush at depths of ≥ 5 km. At slower spreading rates, loss of heat by conduction was too great to produce a steady-state magma chamber. Although quite illustrative of the processes of simultaneous extension and intrusion, this steady-state model does not illustrate how the chamber may grow with time by successive intrusion of magma as ambient temperatures are raised above the intrusion solidus.

Recent work by Hanson and Glazner (1995) built upon Sleep's earlier analytical results by considering the transient evolution of a chamber and utilizing the numerical finite difference approach to incorporate differing magma compositions and simultaneous extension during intrusion in a continental setting. In their formulation, the two-dimensional heat conduction equation includes a spreading rate term (see Carslaw and Jaeger, 1959; Sleep, 1975). Hanson and Glazner (1995) modeled two general spreading scenarios. In the first, crust was allowed to spread at a given rate, heat (magma) entered the extending crust at a constant rate, and temperatures were calculated at the spreading axis. At depths of 8 km, spreading rates of 4 cm year^{-1}, and after addition of 4 km of intruded material, a steady-state chamber was constructed after 90 ka at the spreading axis. The second scenario began with a pre-existing 1 km-wide magma body at the site of emplacement constructed by an unspecified process. Upon further intrusion at spreading rates of 2 cm year^{-1}, ambient temperatures were sufficiently high to maintain a steady-state chamber. In both scenarios, extension and magma emplacement occurred over the entire thickness (depth) of the crustal model (Hanson and Glazner, 1995). Implicit in these models is that a source region must be feeding the pluton over the entire duration of chamber construction, a process which may take up to millions of years for large plutons (e.g. Fleck *et al.*, 1996). Given that dike widths and durations of freezing are related to melt flow velocities (e.g. Lister and Kerr, 1991; Petford *et al.,* 1993), maintaining a continuously flowing *granitic* dike over these time-scales requires (a) rapid and continuous melt extraction from the source region, (b) rapid and continuous flow of *granitic* magma through the growing chamber, and (c) unreasonable volumes of magma at the level of emplacement for a given time increment.

Our model is designed to evaluate the temperature changes during episodic intrusion of dikes, assuming a constant magma supply during pluton construction. We first formulate one- and two-dimensional finite difference methods to solve the heat conduction equation. Rather than using a spreading term in the heat conduction equation, we simulate intrusive spreading by physically translating a portion of the host rocks in the crustal model. We then allow for alteration of the model by intruding melts of different widths at various times while maintaining the stability of the finite difference heat conduction. This intrusion rate-dependent thermal modeling is based on the heat conduction equation which in two dimensions is (e.g. Carslaw and Jaeger, 1959; Bejan, 1993):

$$\frac{\partial^2 T}{\partial x^2}+\frac{\partial^2 T}{\partial z^2}=\frac{1}{k}\frac{\partial T}{\partial t} \qquad (1)$$

where T is temperature, t is time, x and z are the horizontal and vertical coordinates, respectively, and k is the thermal diffusivity, which equals $K/\rho c$, where K is the thermal conductivity, ρ is the density, and c is specific heat capacity. Input variables for these and other parameters that were used in the models are included in Table 1.

Table 1. Input variables for two-dimensional models*

Initial melt temperature, T_m	850°C
Initial host rock temperature, T_c	0–950°C
Melt density, ρ_m	2400 kg m^{-3}
Host rock density, ρ_c	2670 kg m^{-3}
Melt thermal conductivity, K_m	3.05 W m^{-1}K^{-1}
Host rock thermal conductivity, K_c	2.65 W m^{-1}K^{-1}
Melt specific heat, c_m	1142 J kg^{-1}K^{-1}
Host rock specific heat, c_c	1000 J kg^{-1}K^{-1}
Melt latent heat, L_m & Temp.	1.5×10^5 J kg^{-1}, 800°C
Host rock latent heat, L_c & Temp.	2.2×10^5 J kg^{-1}, 1000°C
Basal heat flux, q	60 mW m^{-2}

* Values from Hanson and Glazner (1995); Furlong *et al.* (1991).

The finite difference approximation of equation (1) (Croft and Lilley, 1977; Bejan, 1993) utilizes a grid of evenly spaced nodes each of which is allowed to have unique values of physical properties. The heat conduction equation is solved at each node using appropriate initial and boundary conditions for every time step with selected time steps providing output for display. One of five types of boundary conditions (constant temperature, linear temperature gradient, heat flux, ambient temperature convection, and self-absorbing) is set for each side of the model and is implemented at each calculated time step. The effect of latent heat of crystallization is computed using the formulation of Croft and Lilley (1977) whereby at each node the amount of heat stored or released is computed when the nodal temperature passes through the material's (host rock or melt) latent temperature (Table 1). Latent heat of crystallization was released once the melt cooled through 800°C; release of latent heat of fusion occurred in the host rocks when temperatures passed 1000°C. However, in all of the simulations, ambient temperatures never passed 650°C. The time interval between internal calculations of heat conduction is selected in order to maintain stability based on the Fourier number criteria.

The above conventional one- and two-dimensional finite difference thermal conduction methods are modified to allow for the addition of intrusive material and the mechanical translation of the host rock. A portion of the model is translated by a given intrusion width with the new space filled by the intrusion at a specified position, melt temperature, and height (in two dimensions). A corresponding area of host rock is then translated away from the intrusion axis, simulating fault displacement. The time interval between intrusions is governed by the intrusion width and the overall spreading rate, the latter being controlled by fault slip rates. As successive intrusions occur, the older intrusions are translated along with the host rock

away from the intrusion axis. For all simulations, the intrusion axis remains fixed on the left side of the model and the host rocks are translated to the right. This will increase the rate of heating at the intrusion axis as compared to random intrusion over a given area which we did not model. Thus, our estimates of the times necessary to elevate ambient temperatures above the intrusion solidus will be minimum values.

Processes such as magma convection and hydrothermal circulation will affect the nature of heat transfer and cooling of the intrusion (Spera, 1980). We assume that chamber-wide convection is not a significant process governing the advection of heat through the intrusion–host rock system at the level of emplacement (see below), a contention supported by theoretical and observational data (Marsh, 1989; Clemens and Mawer, 1992). We have not incorporated endothermic contact metamorphic reactions nor hydrothermal circulation in the host rocks. While we acknowledge the effect that these processes may have in the convection of heat away from intrusions in shallow crustal environments, our modeling evaluates purely conductive cooling for three reasons: (1) we are interested in minimum estimates for the length of time necessary to construct a steady-state magma chamber, and the above processes will increase these estimates; (2) the time scale of initiation of heat loss by hydrothermal convection may be of the order of 10^5–10^6 years (Marsh, 1990) and so will probably not affect the durations needed to reach hypersolidus ambient conditions (see below); and (3) many plutons are known to have cooling histories that are compatible with pure conductive heat transfer (Parmentier and Schedl, 1981; Bowers *et al.*, 1990; Barton *et al.*, 1991).

Two-dimensional models

The two-dimensional model dimensions are 400×400 nodes, which at 100 m per node yields a 40 km $\times$ 40 km model, consistent with the dimensions of the continental crust and closely spaced enough to model many igneous intrusions (see below). In order to simulate a stable and realistic ambient background temperature a positive heat flux at the base (60 mW m^{-2}) and a negative (but identical) heat flux at the top of the model is superposed on an initial top to bottom gradient of 0–950°C. The sides of the model are set with an absorbing boundary condition. We acknowledge the non-linear effect on the geotherm of radiogenic heat-producing elements in the crust, but simplify the means of modeling the overall ambient heat budget in the crust by using the above approach. Models were run at total slip rates of 10, 25, and 50 mm $year^{-1}$. Final two-dimensional intrusion dimensions vary in vertical and horizontal dimensions between (a) 10 km $\times$ 5 km tabular intrusions emplaced between 5–10 km depth and 15–20 km depth, (b) 10 km $\times$ 10 km squares emplaced between 5 and 15 km depth, and (c) 5 km $\times$ 10 km rectangles emplaced between 5 and 10 km depth.

Instantaneous vs successive intrusion

With the exception of Hanson and Glazner (1995), most numerical models of heat transfer during magma emplacement have assumed instantaneous intrusion and then calculated the thermal decay with time and distance (e.g. Bowers *et al.,* 1990). However, an instantaneously emplaced pluton may not display the same characteristics as a pluton constructed by a series of smaller events distributed over time even when the total volumes of mass and heat addition are the same. The difference is that episodic emplacement allows incremental volumes of magma to be emplaced in the crust at a given time-step. Figure 2 compares the conductive cooling of two identically shaped bodies, one intruded instantaneously (Fig. 2a) and the other (Fig. 2b) constructed over 200 ka by successive emplacement of 100 m dikes by a fault-controlled model. Note that at 200 ka, when both intrusions begin their pure conductive cooling phase, the instantaneously intruded body (Fig. 2a) generates a larger heat flux into the host rocks resulting in higher temperatures distributed immediately adjacent to the intrusion. However, modeling instantaneous emplacement at some level in the crust ignores the effects that earlier magmatism may have on the growth of the intrusion with time and the resulting temperature distribution at the emplacement site. From 0 to 200 ka isotherms migrate away from the intrusion axis centered at 10 km during successive intrusion (Fig. 2b). Once intrusion ceases, the isotherms begin to converge back on the center of the intrusion. This illustrates the compet-

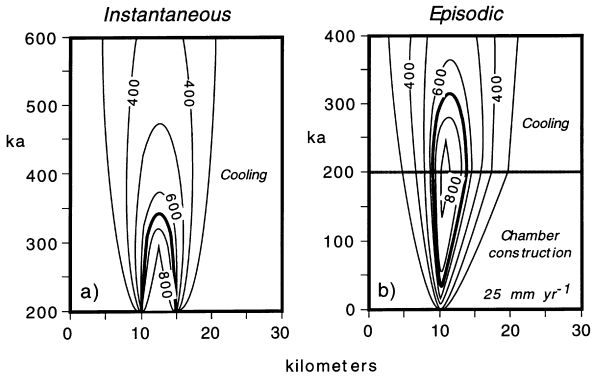

Fig. 2. Comparison of time-dependent nature of conductive cooling for (a) an intrusion instantaneously emplaced at 200 ka, and (b) construction of the same size intrusion by emplacement of successive dikes at a spreading rate of 25 mm $year^{-1}$. Bold black line is the 650°C wet granite solidus; isotherms are contoured every 100°C. Intrusion axis is at 10 km and the intrusion grows to a width of 5 km. (b) Intrusion growth between 0 and 200 ka; after 200 ka intrusion ceases and the body conductively cools. Note that the initial heat flux from the instantaneously emplaced intrusion is higher immediately adjacent to the intrusion in (a) and that during construction of the magma chamber in (b) isotherms migrate away from the intrusion axis.

ing interplay between cooling processes at the intrusion–host rock contact and heating processes at the axis of intrusion. This interplay is principally controlled by the episodicity of intrusion which is a function of spreading rate.

RESULTS

Figure 3 is an example of the two-dimensional thermal results for the construction of a granite intrusion emplaced as individual 100 m dikes into granodiorite host rocks displaced at 25 mm year^{-1} using boundary conditions described above. At each time step a new dike is emplaced at the left edge of the intrusion and the host rocks, including previously intruded material, are translated away from the intrusion axis. Each panel in Fig. 3 represents 40 ka with the last reflecting thermal conditions after 400 ka. At the end of the run the intrusion forms a square-shaped body occupying a 10 km $\times$ 10 km area between 5 and 15 km depth in the crust. The 650°C granite wet solidus isotherm is also contoured in Fig. 3 and represents in this model a simplified boundary separating solidified material from partially molten material (see Discussion).

Shallow- and mid-crustal tabular intrusions

Figure 4(a–c) displays the results of three simulations produced by intruding 100 m dikes at different spreading rates forming 10-km-long tabular intrusions in the shallow crust (5–10 km depth, inset Fig. 4a). These plots show the solidus and subsolidus isotherms and the location of the intrusion–host rock contact as a function of time and distance from the intrusion axis (origin). Each plot displays the evolution of temperature (distance–time) measured from the center of the intrusion outward into the host rocks over the entire time of the simulation. Note that the temperatures as a function of time and distance are maximum values for the individual models. Similar plots through the upper or lower portions of the intrusion will yield lower temperatures for a given distance and time. For example, Fig. 4(a) shows how the solidus isotherm and intrusion–host rock contact will migrate away from the intrusion axis with time at a depth of 7.5 km and spreading rate of 10 mm year^{-1}. The dotted portion of the solidus isotherm in Fig. 4(a & b) indicates that the ambient temperatures were elevated and then cooled through 650°C creating an ephemeral solidus. The geologic result of this phenomenon is formation of a sheeted complex. The bold portion of the isotherm denotes temperatures that remain at 650°C. Figure 4(d–f) shows the same features at 17.5 km depth in the center of a tabular pluton emplaced in the mid-crust (15–20 km depths, inset Fig. 4d). For tabular intrusions emplaced in the shallow crust with slip rates less than 10 mm year^{-1} (Fig. 4a), a constant 650°C isotherm is not attained even after 1 Ma implying that intrusions constructed in this fashion will form sheeted complexes. With faster spreading rates, the time necessary to construct a steady-state magma chamber above its solidus decreases to ~55 ka at 25 mm year^{-1} and < 10 ka at 50 mm year^{-1} (Fig. 4b & c). Tabular intrusions constructed by displacement along faults at mid-crustal depths need much less time to elevate ambient temperatures above the wet granite solidus even at slow spreading rates of 10 mm year^{-1} (Fig. 4d–f). Table 2 summarizes the length of time necessary to construct a stable magma chamber above its solidus as a function of spreading rate, intrusion size, and depth of emplacement for this study.

Square and rectangular intrusions

The results of varying intrusion geometry by modeling square and rectangular intrusions emplaced between 5 and 15 km depth indicate that, at spreading rates of 10 mm year^{-1} or less, it may take a minimum of ~350 ka (Fig. 5a) and ~260 ka (Fig. 5d), respectively, before ambient temperatures of 650°C are reached. At faster spreading rates, this time dramatically decreases: for a square intrusion the constant 650°C isotherm is reached in < 30 ka at 25 mm year^{-1} and < 10 ka at 50 mm year^{-1} (Fig. 5b & c; Table 2). Figure 5(b) shows how the isotherms migrate away from the intrusion axis with time for the model shown in Fig. 3.

Migrating solidus isotherm

Figures 6 and 7 show how the solidus isotherm migrates with time for the different intrusion dimensions and the evolution of the position of the intrusion–host rock contacts as a function of spreading rate. The dotted portion of the isotherm indicates when the temperature briefly peaked above 650°C during each intrusion event but then quickly cooled through the solidus. At slip rates of 10 mm year^{-1}, a tabular intrusion emplaced at 5–10 km will never reach ambient temperatures above the solidus and will consist entirely of sheeted dikes (Fig. 6a). At faster spreading rates the ambient temperatures quickly reach the solidus and sheeted dikes make up only a small fraction (< 10%) of the total intrusion at the end of the model run (Fig. 6b & c). Intrusions with the same dimensions emplaced in the middle crust require less than 30 ka at 10 mm year^{-1} to pass the solidus (Fig. 6d). At higher spreading rates, temperatures rise rapidly and the 650°C isotherm migrates into the sheeted dikes during the early stages of intrusion (Fig. 6e & f). This is probably due to the combination of higher ambient temperatures as well as a strong but transient initial temperature gradient which allows the heat to move at a faster rate at the onset of intrusion.

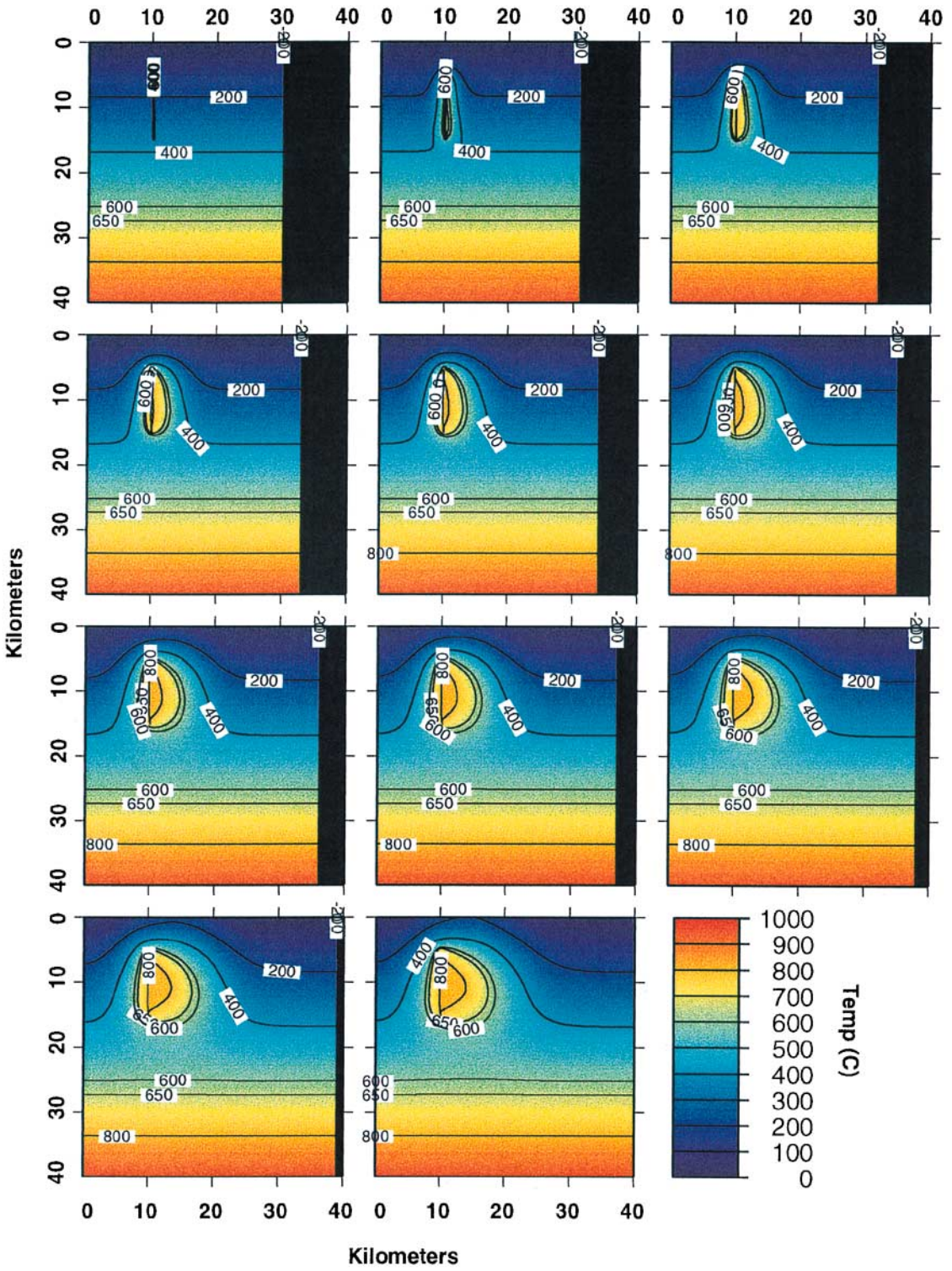

Fig. 3. Example of two-dimensional thermal results of emplacement of 100 m granite dikes intruded over time into granodioritic crust forming a 10 km × 10 km (square) intrusion after 400 ka. Each panel represents 40 ka with the initial panel at 0 ka. The 650°C contour represents the wet granite solidus which we define as the boundary between crystallized and magmatic intrusive material (see text). The black belt along the right margin represents the total growth of the model through time; during each intrusion, the host rocks are translated to the right by the width of the intrusion. Space above and below the intrusion is then filled with host rock material with diffusivity (k) values identical to the adjacent nodes. Note the asymmetry of temperature distribution with time.

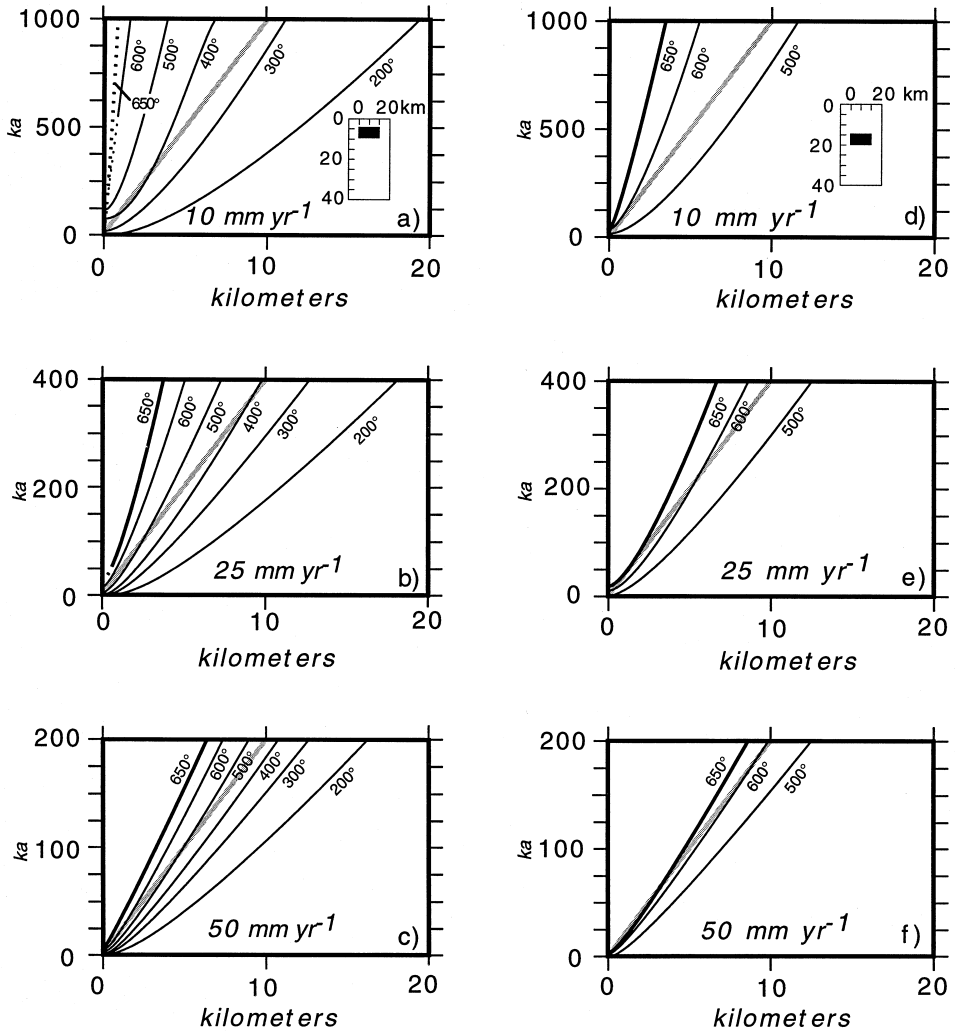

Fig. 4. (a–c) Evolution of isotherms for a 10-km-long tabular intrusion of granite composition emplaced between 5 and 10 km into granodioritic crust at 10, 25 and 50 mm year^{-1} spreading rates. Position of isotherms is measured relative to the intrusion axis (0 km) and through the center of the intrusion in cross-section (7.5 km depth). Dotted lines represent 'ephemeral' isotherms (see text). Linear gray lines represent the migration of the contact between the intruded material and the host rocks with time, the slope of which equals the spreading rate. The bold portion of the isotherm denotes temperatures that remain at 650°C. Inset diagram in (a) shows the crustal model and the intrusion dimensions at the end of each model run for this simulation. (d–f) Isotherms for a 10-km-long tabular intrusion of granite composition emplaced between 15 and 20 km into granodioritic crust at 10, 25, and 50 mm year^{-1} spreading rates. Position of isotherms is measured relative to the intrusion axis (0 km) and through the center of the intrusion in cross-section (17.5 km depth). Inset diagram in (d) shows the crustal model and the intrusion dimensions at the end of each model run for this simulation.

Table 2. Summary of two-dimensional results: time necessary to reach intrusion solidus as a function of spreading rate and intrusion dimensions

Spreading rate	Intrusion shape & size (vertical × horizontal)	Level of emplacement	Time to sustain temperatures above 650°C	Width of sheeted dikes normalized to intrusion L
10 mm year^{-1}	Tabular 5 km × 10 km	5–10 km	> 1 Ma	1
10 mm year^{-1}	Square 10 km × 10 km	5–15 km	~350 ka	0.25
10 mm year^{-1}	Rectangle 10 km × 5 km	5–15 km	~260 ka	0.30
10 mm year^{-1}	Tabular 5 km × 10 km	15–20 km	< 30 ka	< 0.10
25 mm year^{-1}	Tabular 5 km × 10 km	5–10 km	~55 ka	0.10
25 mm year^{-1}	Rectangle 10 km × 5 km	5–15 km	~48 ka	< 0.10
25 mm year^{-1}	Square 10 km × 10 km	5–15 km	~30 ka	< 0.10
25 mm year^{-1}	Tabular 5 km × 10 km	15–20 km	< 25 ka	< 0.10
50 mm year^{-1}	Tabular 5 km × 10 km	15–20 km	< 10 ka	$\ll$0.10
50 mm year^{-1}	Square 10 km × 10 km	5–15 km	< 10 ka	$\ll$0.10
50 mm year^{-1}	Tabular 5 km × 10 km	5–10 km	< 10 ka	$\ll$0.10
50 mm year^{-1}	Rectangle 10 km × 5 km	5–15 km	< 10 ka	< 0.10

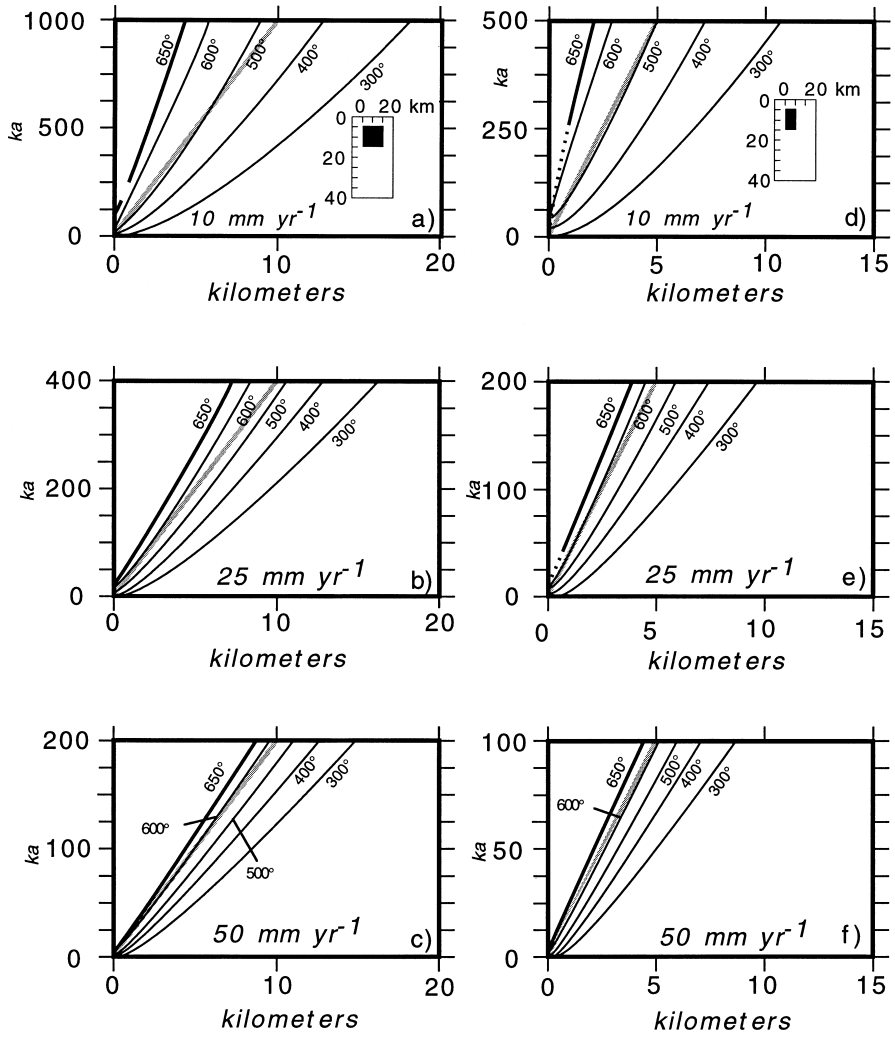

Fig. 5. (a–c) Evolution of isotherms for a 10 km × 10 km square intrusion of granite composition emplaced between 5 and 15 km depth into granodioritic crust at 10, 25 and 50 mm year^{-1} spreading rates. Position of isotherms is measured relative to the intrusion axis (0 km) and through the center of the intrusion in cross-section (10 km depth). Inset diagram in (a) shows the crustal model and the intrusion dimensions at the end of each model run for this simulation. (b) Time–space migration of isotherms at 10 km depth from Fig. 3. (d–f) Isotherms for a 5 km × 10 km vertical, rectangular intrusion of granite composition emplaced between 5 and 15 km depth into granodioritic crust at 10, 25, and 50 mm year^{-1} spreading rates. Position of isotherms is measured relative to the intrusion axis (0 km) and through the center of the intrusion in cross-section (10 km depth). Inset diagram in (d) shows the crustal model and the intrusion dimensions at the end of each model run for this simulation. Legend same as Fig. 4.

One significant result of this study is that once ambient temperatures are elevated above the solidus isotherm, further intrusion of magma may no longer form a sheeted margin. Figures 6 and 7 show the distribution of hypersolidus material and solidified dikes as a function of spreading rate. Prior to reaching the 650°C isotherm melts will solidify and form dikes. As temperatures increase and the 650°C isotherm is passed the formation of sheeted intrusions will cease and subsequent intrusions will remain at hypersolidus conditions, assuming constant spreading and intrusion rates. At this point the width of the zone of sheeted intrusions is frozen and the newly emplaced magmas will remain at hypersolidus conditions; this boundary is denoted by a dash–dot line in Figs 6 and 7. However, because the velocity of spreading is greater than that of the migrating solidus, as the reservoir continues to grow, material that intruded above the 650°C isotherm will eventually migrate across the solidus. For example, in a traverse of Fig. 7(a) at 750,000 years, material left of the 650°C isotherm will remain in a magmatic state (hatch pattern in Fig. 7a), material between the 650°C isotherm and the dash–dot line will have intruded above the 650°C but cooled through the solidus, and material between the dash–dot line and the host rock contact will be sheeted. The actual boundary separating these different zones may be gradational or cryptic in the field (McNulty *et al.*, 1996). Note that for spreading rates ≤10 mm year^{-1} a significant portion of the total intrusion will contain sheets (Fig. 7a & d); chambers formed during spreading rates of 25 mm year^{-1} also contain sheets but may form

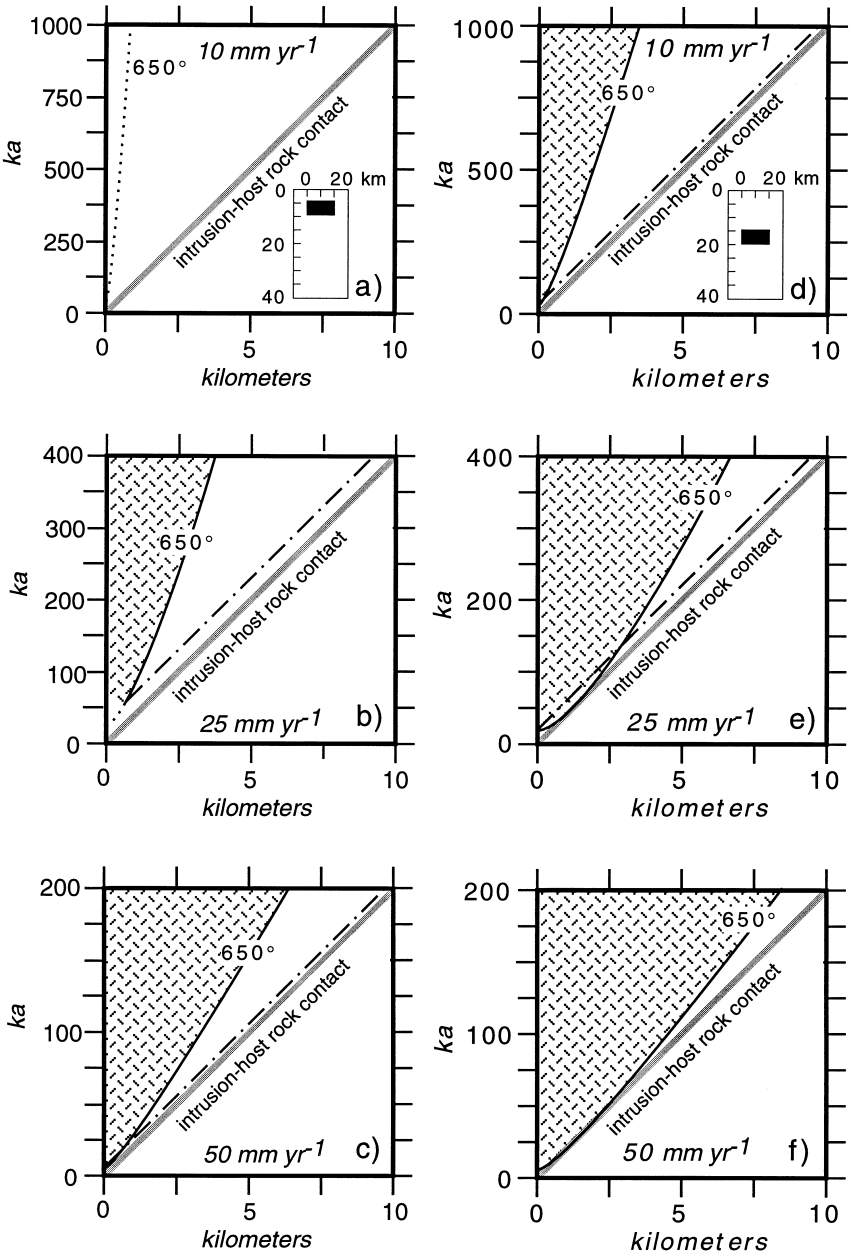

Fig. 6. (a–f) Plot of solidus isotherms for 5 km × 10 km tabular intrusions emplaced at 5–10 km depth (a–c), and 15–20 km depth (d–f), as a function of time. Position of isotherms is measured from the intrusion axis (0 km) and through the center of the intrusion cross-section. Dotted line = ephemeral solidi; dashed–dotted line = boundary between portion of intrusion forming sheeted dikes and crystallized 'homogeneous' magma that was emplaced at ambient temperatures above the solidus and then cooled through the solidus with time; hatch pattern = hypersolidus granitic magma; gray line represents the contact between the growing intrusion and the host rock which tracks the spreading rate (distance/time).

$<10\%$ of the total intrusion (Figs 7b & e). Only at 50 mm year^{-1} is sheeting not preserved along the margins of magma chambers by fault-controlled models (Figs 6f & 7c). The widths of sheeted dikes normalized to the total intrusion width are summarized in Table 2.

DISCUSSION

From Table 2 it is apparent that magma reservoirs constructed in a fault-controlled setting will attain ambient temperatures greater than their solidus relatively quickly at spreading rates greater than 50 mm year^{-1}. Even at slower spreading rates of 25 mm year^{-1} the time necessary to pass the magma solidus is less than the uncertainties of most geochronometric dating. With the exception of the mid-crustal simulation (Fig. 4d), spreading rates $\leq$10 mm year^{-1} are likely to produce reservoirs that contain significant portions of solidified material that retain their initial sheeted characteristics. This does not necessarily mean, however, that fault-controlled models can produce large,

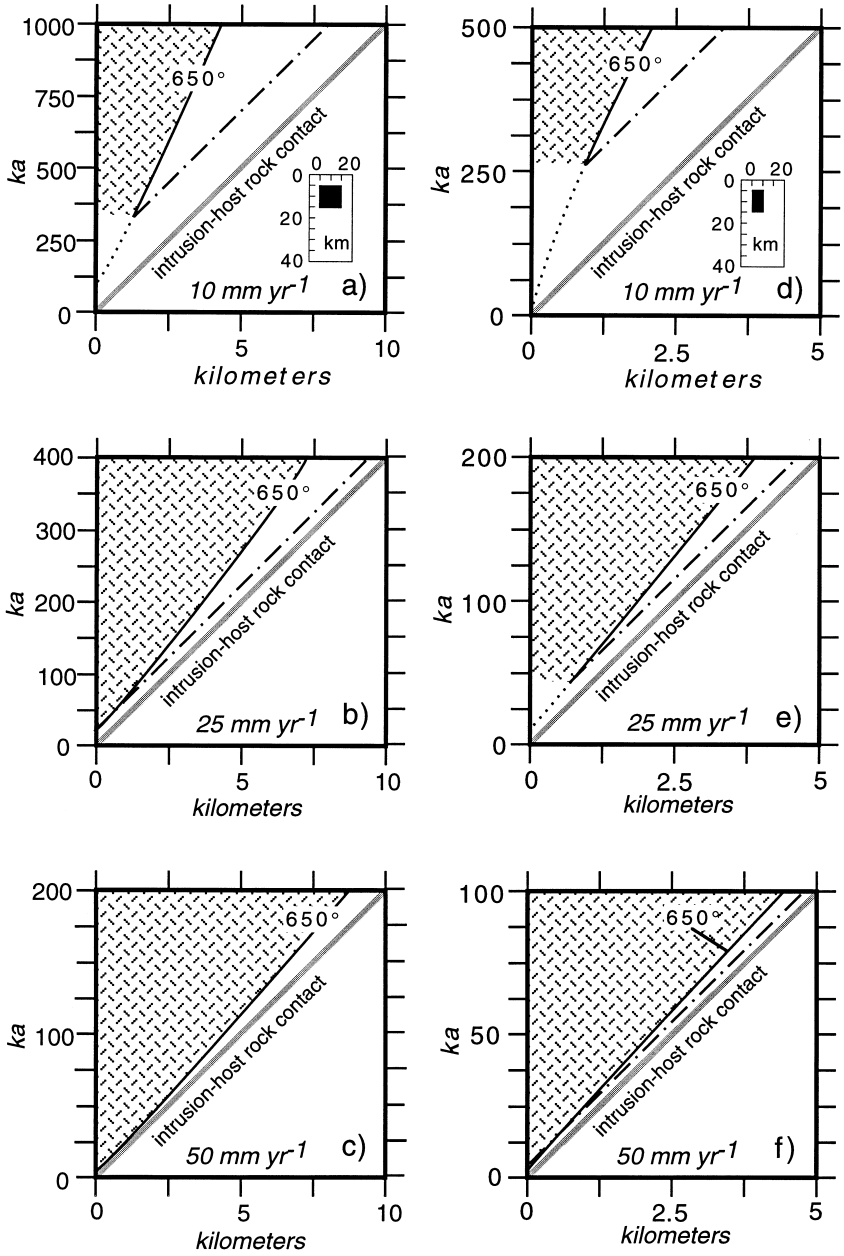

Fig. 7. (a–f) Plot of solidus isotherms for 10 km × 10 km square intrusions (a–c), and vertical rectangular 5 km × 10 km intrusions (d–f), both emplaced between 5-15 km depth, as a function of time. Position of isotherms is measured from the intrusion axis (0 km) and through the center of the intrusion cross-section. Legend same as Fig. 6.

zoned, non-sheeted intrusions. In the following discussion we explore a number of effects that may act to alter the thermal evolution of the fault models with time. These include changes in host rock ambient temperatures and magma composition, hydrothermal circulation, three-dimensional heat transfer, and whether or not the slip rates modeled are geologically appropriate. Finally, we evaluate the implications of the construction of fault-controlled bodies for magma chamber dynamics.

Effects of ambient temperatures and magma composition

The modeling incorporates parameters that are appropriate for melts of granite composition with a wet solidus at 650°C and an initial emplacement temperature of 850°C. Altering the diffusivities (k) in equation (1) and initial melt temperatures to more intermediate composition values (e.g. tonalite or granodiorite) will effectively raise the heat budget of the system. However, these compositions will have corre-

spondingly higher solidi and thus will still need sufficient time to elevate the ambient temperatures above their solidi. We are currently addressing the role that varying composition will have on the rate of formation of hypersolidus magma chambers. Our initial results indicate that the rates of heat transfer may scale accordingly with composition (see also Furlong *et al.*, 1991; Hanson and Glazner, 1995).

A major effect that will control the rate of conductive heat transfer is the initial temperature difference between the host rock and melt. This effect is illustrated by comparing results in Fig. 4. In Fig. 4(a–c), a tabular intrusion was constructed in the shallow crust (5–10 km) with corresponding host rock temperatures ranging from 200 to 300°C, whereas in Fig. 4(d–f) a tabular intrusion with the same dimensions was constructed in the mid-crust (15–20 km) at host rock temperatures ranging from 400 to 500°C. At spreading rates of 10 mm year^{-1}, the shallow crustal example (Fig. 4a) never reached constant solidus temperatures after 1 Ma. However, at mid-crustal depths it took less than 30 ka to pass solidus temperatures for the same spreading rate. Besides level of emplacement, depth-dependent changes in the geothermal gradient may affect the thermal behavior of vertically extensive intrusions. In Fig. 3, the temperature distribution with time becomes asymmetric about the intrusion due to the combined effects of continued extension and higher ambient temperatures with depth. Because temperatures increase with depth due to the ambient geothermal gradient, profiles through the lower portion of the intrusion have lower heat fluxes and show correspondingly higher temperatures, although still less than through the center of the intrusion (Fig. 3).

The models do not account for transient surface warming due to volcanism and the generation of additional heat from a source conduit or the site of melt generation. This problem was circumvented by constructing a geothermal gradient that approximates regional metamorphic P–T–t conditions observed near shallow to mid-crustal intrusions (e.g. Bateman, 1992) while ignoring the causes of this heat generation. Additional heat from the source conduit should have second order effects on the temperature distribution around the intrusions.

Effects of three-dimensional heat transfer

We have constructed the models in two dimensions because of the inherent complexities (and longer computing times) of three-dimensional modeling. An important assumption in two-dimensional modeling is that the model intrusions, and therefore heat conduction, are allowed to extend infinitely in the third dimension. The result of this is to overestimate the amount of heat in the system (Furlong *et al.*, 1991). In our modeling we have used simple intrusion geometries which extend easily into the third dimension. However, the temperature values obtained are maximum and it may require longer durations of intrusion and spreading before solidus temperatures are reached.

Effects of hydrothermal circulation

We have assumed only conductive heat transfer for intrusion cooling. Convective hydrothermal circulation within the host rocks can lead to increased intrusion cooling rates (e.g. Cathles, 1981), which would require the fault-controlled emplacement models to have much faster spreading rates if they are to produce chambers with ambient temperatures above the solidus. Marsh (1990) and Furlong *et al.* (1991) calculated the time necessary to develop full-scale convective hydrothermal flow and associated heat loss in the host rocks to be on the order of $>10^5$ year and possibly much greater depending on the temperature gradient in the intrusion–host rock system and host rock permeability. In the numerical models presented above, temperatures are continually rising due to the successive input of magma which is likely to suppress up-temperature gradient fluid fluxes from the host rocks, if they exist. Furthermore, Cathles (1981; see also Parmentier and Schedl, 1981; Furlong *et al.*, 1991) showed that conductive heat flow across the intrusion–host rock contact in arc settings is not significantly affected by fluid circulation in the host rocks and that crystallization and cooling rates remain relatively unchanged until the body was significantly crystallized, fractured, and permeable to fluid flow.

What are reasonable slip rates in orogenic settings?

Given that many of the intrusions that are hypothesized to have been emplaced by fault models are largely free of sheeted margins and contain chamber-wide magmatic foliation patterns (e.g. Tikoff and Teyssier, 1992), the modeling indicates that slip rates must be fairly rapid ($\geq$50 mm year^{-1}) to produce such plutons or multiple emplacement processes were active. Is this a geologically reasonable slip rate for a syn-batholithic fault zone? Compiled strike-slip rates from modern volcanic arcs calculated from plate motion vector residuals (Jarrard, 1986) give a range of values between 0 and $<$40 mm year^{-1}, increasing with the obliquity of convergence. Paterson and Tobisch (1992) compiled a variety of rates that may affect magmatic arc evolution and used 30 mm year^{-1} as an average slip rate for arc-parallel faults. Slip rates in other tectonic environments tend to be slower; estimates from fold and thrust belts and extensional metamorphic core complexes range from 2–16 to $\sim$23 mm year^{-1}, respectively (Hacker *et al.*, 1990; Paterson and Tobisch, 1992). A realistic range for average slip rates on faults in arc environments may therefore be 10–30 mm year^{-1}. The time values in our modeling (Table 2) are minimum estimates, and thus we predict that plutons constructed

by fault models in regions with low to moderate ambient temperatures should display significant sheeted margins.

Migrating solidification fronts

The models clearly show that episodic magma emplacement will have a very different effect on the spatial and temporal evolution of the solidus than instantaneous emplacement. Even if not emplaced by a fault-controlled model, many intrusions display evidence that they were constructed by transient multiple pulses of magma (e.g. Paterson and Vernon, 1995; Fleck *et al*., 1996; McNulty *et al*., 1996). Figures 6 and 7 demonstrate that the velocity of the migrating intrusion–host rock contact, which equals the spreading rate, is greater than the velocity of the migrating solidus; the latter velocity being a function of both the cooling rate and the intrusion rate. Because faster spreading rates are balanced by greater addition of magmatic material at the intrusion axis, the velocity of the solidus isotherm may approach the spreading rate if ambient conditions are appropriate (e.g. Figs 6f, 7c & f). In effect, repeated intrusion of hot material at the intrusion axis acts to retard the rate of solidus migration back towards the center of the intrusion. Therefore, once the 650°C isotherm is reached and intrusion continues at a comparable rate a steady-state chamber will be maintained whose size at any given time will be smaller than the total intrusion size, a conclusion also reached by Hanson and Glazner (1995).

By emphasizing the solidus isotherm we are establishing the minimum temperature where a steady-state chamber may form. We acknowledge that the zone immediately up temperature from the solidus is a rheologically complex crystal–melt mush. This zone, the solidification front, will occur between the solidus and below-liquidus isotherms and will contain a range of crystal–melt ratios (Marsh, 1995; Barboza and Bergantz, 1996). The curving nature of the solidus isotherm with time (Figs 2 & 3) also indicates that although material may initially intrude a growing reservoir as sheets or dikes, the solidification front may evolve to be curviplanar. This occurs because the rate of intrusion heat loss is faster along sharp corners than flat sides due to more intrusion surface area per intrusion volume in contact with the host rocks at the corners of the intrusive body (Furlong *et al*., 1991; Bejan, 1993). This drives isotherms towards inwardly migrating circular or elliptical patterns (in two dimensions) with time. If the solidification front becomes more circular with time, physical processes that occur within this front may produce structures that reflect this curvature. For example, continued intrusion of magma pulses may cause magma surges, that upon entering the chamber, will undergo divergent flow, producing flattening strains parallel to the advancing solidification front. This may be one explanation for the commonly observed 'onion-skin' magmatic foliation pattern observed in many plutons, and may be independent of the mechanism of intrusion.

Migrating solidification fronts in a cooling intrusion will lead to diachronous formation of igneous and/or solid-state structures such as foliations which form when individual crystals mechanically interact (melt fractions $\ll$55%). As the solidus isotherm migrates away from the intrusion axis, as in Figs 6 and 7, the solidification front will track this outward migration. This could potentially result in magmatic (and solid-state) fabric development during both the construction and cooling of the intrusion. Once ambient temperatures are elevated above the solidus, intrusions may continue to be emplaced as dikes but their margins will be indistinguishable in the field, or may be allowed to entirely mix with adjacent similar or identical composition magmas. At this state, although cryptic compositional layering may be preserved, magmatic foliations may become realigned by a number of different processes (e.g. Fowler and Paterson, 1997), may or may not have the same geometry as foliations formed earlier along the margins of the intrusion, and may cross-cut compositional boundaries.

Lastly, we note that if the hypersolidus magma chamber begins its life with small dimensions, grows steadily as new magma is intruded, but is always smaller than the total intrusion, one implication is that earlier emplaced magmas will not be in chemical 'communication' with later magmas. This may limit the degree to which differentiation and mixing may occur at the site of emplacement.

CONCLUSIONS

Numerical simulations indicate that magma emplacement into a fault-controlled setting is a thermally viable means of constructing a large igneous body such as a pluton, but the margins of the intrusion should contain sheeted dikes. Because many of the intrusions hypothesized to have been emplaced by such models do not display the features predicted by our simulations and field considerations (e.g. Paterson and Fowler, 1993), we urge caution in ascribing a fault-controlled model for pluton emplacement. One general conclusion of this study is that the thermal and mechanical behavior of the intrusion host rock system, when intrusion occurs episodically through time, is very different from that of instantaneous intrusion. Because it is unlikely that most large intrusions were formed instantaneously, we contend that the effects of continued addition of heat on the migration of solidification fronts may have implications for magmatic processes in a variety of emplacement scenarios. We summarize the following results of our modeling and their implications.

1. For spreading rates $\leq$10 mm year^{-1}, construction of a steady-state magma chamber in the shallow crust did not commence until after 260 ka (rectangular), 360 ka (square), and 1 Ma (tabular). At mid-crustal conditions it took less than 30 ka for the ambient temperatures to pass the intrusion solidus at a spreading rate of 10 mm year^{-1}. For these spreading rates the intrusions contained from 10 to 100% sheeted dike.
2. At spreading rates of 25 mm year^{-1} ambient temperatures pass the solidus isotherm forming a steady-state reservoir in the range from 55 ka to less than 25 ka, depending on intrusion depth and size. At this rate a dike complex occupies $\leq$10% of the intrusion.
3. Spreading rates of 50 mm year^{-1} may form a stable chamber in less than 10 ka at all depths and sizes. At this rate a dike complex occupies $<$10% of the intrusion.
4. When additional magma is added to the reservoir, solidification fronts may move away from the center of the intrusion tracking the outward migrating solidus isotherm and will become progressively more curviplanar in two dimensions.
5. Steady-state magma chambers constructed by fault-controlled processes will be smaller than the total intrusion, thus magmatic fabrics will form diachronously as they become frozen in during migration of the solidification front.
6. Plutons constructed by the fault-controlled process may not show significant comagmatic differentiation trends developed at the site of emplacement.

Acknowledgements—We thank Drs Sandy Cruden, Keith Benn, and Ed Sawyer for convening the 1997 GAC Symposium on Extraction, Transport, and Emplacement of Granitic Magmas where the origins of this paper were presented; Greg Davis, Christine Carlson, Dave Bowman, Keegan Schmidt, and Brendan McNulty for engaging discussions which helped clarify many of the ideas presented. Ed Sawyer reviewed and shepherded an earlier draft of the manuscript through *JSG*; candid reviews by George Bergantz and Brooks Hanson substantially added to the presentation and implications of the science. ASY thanks Keegan Schmidt for an eleventh hour review, Ken Fowler for his concise insights on plutons, and Celeste Thomson for inspiration, encouragement and patience over the past seven years. Thanks also to Barrie Clarke and the Granite-Net for stimulating dialogue and bantering across the oceans. Early work on this project was funded by NSF Grant EAR-8916325 (to Scott R. Patterson).

REFERENCES

Barboza, S. A. and Bergantz, G. W. (1996) Dynamic model of dehydration melting motivated by natural analogue: applications to the Ivrea–Verbano zone, northern Italy. *Transactions of the Royal Society of Edinburgh: Earth Sciences* **87,** 23–32.

Barton, M. D., Staude, J. M., Snow, E. A. and Johnson, D. A. (1991) Aureole systematics. *Reviews in Mineralogy* **26,** 723–847.

Bateman, P. C. (1992) Plutonism in the central part of the Sierra Nevada batholith, California. *U. S. Geological Survey Professional Paper* **1483,** 186.

Bejan, A. (1993) *Heat Transfer*. John Wiley & Sons, Inc., New York.

Bowers, J. R., Kerrick, D. M. and Furlong, K. P. (1990) Conduction model for the thermal evolution of the Cupsuptic aureole, Maine. *American Journal of Science* **290,** 644–665.

Carslaw, H. S. and Jaeger, J. C. (1959) *Conduction of Heat in Solids*. Oxford Science Publications.

Cathles, L. M. (1981) Fluid flow and genesis of hydrothermal ore deposits. *Economic Geology*, 75th Anniversary Volume, 424–457.

Clemens, J. D. and Mawer, C. K. (1992) Granitic magma transport by fracture propagation. *Tectonophysics* **204,** 339–360.

Croft, D. R. and Lilley, D. G. (1977) *Heat Transfer Calculations Using Finite Difference Equations*. Applied Science Publishers, London.

Ferre, E., Gleizes, G., Bouchez, J. L. and Nnabo, P. N. (1995) Internal fabric and strike-slip emplacement of the Pan-African granite of Solli Hills, northern Nigeria. *Tectonics* **14,** 1205–1219.

Fleck, R. J., Kistler, R. W. and Wooden, J. L. (1996) Geochronological complexities related to multiple emplacement history of the Tuolumne intrusive suite, Yosemite National Park, California. *Geological Society of America, Abstracts with Programs* **28,** 65.

Fowler, T. K. and Paterson, S. R. (1997) Timing and nature of magmatic fabrics from structural relations around stoped blocks. *Journal of Structural Geology* **19,** 209–224.

Furlong, K. P., Hanson, R. B. and Bowers, J. R. (1991) Modeling thermal regimes. *Reviews in Mineralogy* **26,** 437–505.

Grocott, J., Brown, M., Dallmeyer, R. D., Talor, G. K. and Treloar, R. J. (1994) Mechanisms of continental growth in extensional arcs: An example from the Andean plate-boundary zone. *Geology* **22,** 391–394.

Guineberteau, B., Bouchez, J. L. and Vigneresse, J. L. (1987) The Mortagne granite pluton (France) emplaced by pull-apart along a shear zone: Structural and gravimetric arguments and regional implications. *Geological Society of America Bulletin* **99,** 763–770.

Hacker, B. R., Yin, A., Christie, J. M. and Snoke, A. W. (1990) Differential stress, strain rate, and temperature of mylonitization in the Ruby Mountains, Nevada: Implications for the rate and duration of uplift. *Journal of Geophysical Research* **95,** 8569–8580.

Hanson, R. B. and Glazner, A. F. (1995) Thermal requirements for extensional emplacement of granitoids. *Geology* **23,** 213–216.

Hutton, J. (1794) Observations on granite. *Transactions of the Royal Society of Edinburgh* **3,** 77–81.

Hutton, D. H. W. (1988a) Igneous emplacement in a shear-zone termination: The biotite granite at Strontian, Scotland. *Geological Society of America Bulletin* **100,** 1392–1399.

Hutton, D. H. W. (1988b) Granite emplacement mechanisms and tectonic controls: inferences from deformation studies. *Transactions of the Royal Society of Edinburgh: Earth Sciences* **79,** 245–255.

Jaeger, J. C. (1968) Cooling and solidification of igneous rocks. In *Basalts*, eds H. Hess and A. Poldervaart, Vol. 2, pp. 503–536. The Poldervaart Treatise on Rocks of Basaltic Composition.

Jarrard, R. D. (1986) Relations among subduction parameters. *Reviews of Geophysics* **56,** 217–284.

Karlstrom, K. E., Miller, C. F., Kingsbury, J. A. and Wooden, J. L. (1993) Pluton emplacement along an active ductile thrust zone, Piute Mountains, southeastern California: Interaction between deformational and solidification process. *Geological Society of America Bulletin* **105,** 213–230.

Lister, J. R. and Kerr, R. C. (1991) Fluid-mechanical models of crack propagation and their application to magma transport in dikes. *Journal of Geophysical Research* **96,** 10,040–10,077.

Marsh, B. D. (1989) On convective style and vigor in sheet-like magma chambers. *Journal of Petrology* **30,** 479–530.

Marsh, B. D. (1990) Magma chambers. *Annual Reviews in Earth and Planetary Sciences* **17,** 439–474.

Marsh, B. D. (1995) Solidification fronts and magmatic evolution. *Mineralogical Magazine* **60,** 5–40.

McNulty, B. A., Tong, W. and Tobisch, O. T. (1996) Assembly of a dike-fed magma chamber: The Jackass Lakes pluton, central Sierra Nevada, California. *Geological Society of America Bulletin* **108,** 926–940.

Parmentier, M. and Schedl, A. (1981) Thermal aureoles of igneous intrusions: Some possible indications of hydrothermal convective cooling. *Journal of Geology* **88,** 1–22.

Paterson, S. R. and Tobisch, O. T. (1992) Rates of processes in magmatic arcs: Implications for the timing and nature of pluton

emplacement and wall rock deformation. *Journal of Structural Geology* **14,** 291–300.

Paterson, S. R. and Fowler, T. K. (1993) Extensional pluton-emplacement models: Do they work for large plutonic complexes? *Geology* **21,** 781–784.

Paterson, S. R. and Vernon, R. H. (1995) Bursting the bubble of ballooning plutons: A return to nested intrusion emplaced by multiple processes. *Geological Society of America Bulletin* **107,** 1356–1380.

Petford, N. (1996) Dikes or Diapirs? *Transactions of the Royal Society of Edinburgh: Earth Sciences* **87,** 105–114.

Petford, N., Kerr, R. C. and Lister, J. R. (1993) Dike transport of granitoid magmas. *Geology* **23,** 845–848.

Read, H. H. (1962) Donegal as a natural laboratory for metamorphic geology. *S. K. Roy Commemoration Bulletin of the I. S. M. Geological Society*, Indian School of Mines. Dhanbad, pp. 9–13.

Schmidt, C. J., Smedes, H. W. and O'Neill, J. M. (1990) Syncompressional emplacement of the Boulder and Tobacco Root batholiths (Montana–USA) by pull apart along old fault zones. *Geological Journal* **25,** 305–318.

Sleep, N. H. (1975) Formation of oceanic crust: some thermal constraints. *Journal of Geophysical Research* **80,** 4037–4042.

Spera, F. S. (1980) Thermal evolution of plutons: A parameterized approach. *Science* **207,** 299–301.

Tikoff, B. and Teyssier, C. (1992) Crustal-scale, en échelon "P-shear" tensional bridges: A possible solution to the batholithic room problem. *Geology* **20,** 927–930.